

Measurement of ^4He charge- and mass-changing cross sections on H, C, O, and Si targets in the energy range 70–220 MeV/u for radiation transport calculations in ion-beam therapy

Felix Horst*

*Institute of Medical Physics and Radiation Protection (IMPS), THM University of Applied Sciences Giessen, 35390 Giessen, Germany
and GSI Helmholtzzentrum für Schwerionenforschung, 64291 Darmstadt, Germany*

Giulia Aricò

European Organization for Nuclear Research (CERN), 1211 Geneva, Switzerland

Kai-Thomas Brinkmann

II. Physics Institute, Justus Liebig University, 35392 Giessen, Germany

Stephan Brons

Heidelberg Ion-Beam Therapy Center (HIT), 69120 Heidelberg, Germany

Alfredo Ferrari

European Organization for Nuclear Research (CERN), 1211 Geneva, Switzerland

Thomas Haberer

Heidelberg Ion-Beam Therapy Center (HIT), 69120 Heidelberg, Germany

Andrea Mairani

*Heidelberg Ion-Beam Therapy Center (HIT), 69120 Heidelberg, Germany
and National Centre for Oncological Hadrontherapy (CNAO), 27100 Pavia, Italy*

Katia Parodi

Ludwig Maximilian University (LMU), 80539 Munich, Germany

Claire-Anne Reidel

*GSI Helmholtzzentrum für Schwerionenforschung, 64291 Darmstadt, Germany
and Université de Strasbourg, CNRS, IPHC UMR 7871, 67000 Strasbourg, France*

Uli Weber

GSI Helmholtzzentrum für Schwerionenforschung, 64291 Darmstadt, Germany

Klemens Zink

*Institute of Medical Physics and Radiation Protection (IMPS), THM University of Applied Sciences Giessen, Giessen 35390, Germany;
Department of Radiotherapy and Radiooncology, University Medical Center Giessen-Marburg, Marburg 35043, Germany;
and Frankfurt Institute for Advanced Studies (FIAS), Frankfurt am Main 60438, Germany*

Christoph Schuy

GSI Helmholtzzentrum für Schwerionenforschung, 64291 Darmstadt, Germany



(Received 2 October 2018; published 7 January 2019)

Measured charge- and mass-changing cross sections for the systems $^4\text{He} + ^{12}\text{C}$, $^4\text{He} + ^{16}\text{O}$, $^4\text{He} + ^{28}\text{Si}$, and $^4\text{He} + ^1\text{H}$ in the energy range 70–220 MeV/u are presented. The cross sections were obtained via the attenuation method where a ΔE - E scintillator telescope was used for particle identification. These new data

*Corresponding author: felix.horst@lse.thm.de

have particular relevance for future applications of ^4He ions in ion-beam radiotherapy because this technique relies on precise heavy ion transport models for an accurate dose calculation. The radiation transport codes applied for this purpose typically make use of parametrizations of the total reaction cross section σ_R . The widely used parametrization for nucleus-nucleus reaction cross sections by Tripathi *et al.* is shown to underpredict the new experimental cross sections for ^4He ions in the therapeutic energy range by up to 30%, which can lead to considerable dose calculation uncertainties. Therefore, modifications of the parameters in the Tripathi model are proposed to optimize it for applications related to ^4He ion-beam therapy.

DOI: [10.1103/PhysRevC.99.014603](https://doi.org/10.1103/PhysRevC.99.014603)

I. INTRODUCTION

An essential quantity for heavy ion transport calculations is the total reaction cross section σ_R , which gives the probability for an inelastic nuclear reaction to occur [1,2]. In most Monte Carlo transport codes σ_R is described as a function of the charge and mass of the projectile, the charge and mass of the target and the energy of the colliding system by semiempirical parametric models which are fine-tuned to experimental data. The cross section predictions obtained from these parametrizations are most realistic for colliding systems which are well characterized by experiments. For unexplored systems their predictions might still be reasonable due to the underlying systematics, but for projectile-target combinations of special interest it is preferable to check the models against measured cross sections. The total reaction cross section σ_R is difficult to measure directly because target fragments have very low energies and thus are hard to detect. Typical measured quantities which can serve as an estimate for σ_R are the charge-changing cross section $\sigma_{\Delta Z}$ (projectile loses at least one proton) and the mass-changing cross section $\sigma_{\Delta A}$ (projectile loses at least one nucleon), considering that most nuclear reactions lead to fragmentation of the projectile.

There is a recent interest in radiation transport calculations of ^4He ions in the intermediate energy range because they can be used for ion-beam radiotherapy complementary to the conventionally used protons and ^{12}C ions [3–7]. On the one hand ^4He ions have a sharper lateral dose profile than protons and on the other hand their radiobiology is less complex than for ^{12}C ions. Also the dose tail behind the Bragg peak due to nuclear fragments is less pronounced for ^4He ions than for ^{12}C ions. Furthermore, every synchrotron-based heavy ion therapy facility could in principle be extended to ^4He ion therapy at relatively moderate cost by adding an extra ion source and also cyclotron-based ^4He therapy facilities should be technically feasible. Radiotherapy with ^4He ions had been successfully performed at the Lawrence Berkeley Laboratory until the end of the U.S. heavy ion therapy project in the early 1990s [8,9]. The reintroduction of ^4He ion therapy into radiation oncology is under preparation at the Heidelberg Ion-Beam Therapy Center (HIT) [10–13], where patients have been routinely treated with protons and ^{12}C ions since 2009. Modern scanned ion-beam therapy as performed at HIT uses analytical pencil beam dose calculation algorithms for biological treatment plan optimization [14]. These algorithms require a set of basic input data, preferably for each energy that can be delivered by the accelerator (255 energy steps are available at HIT, ranging from 50–220 MeV/u for ^4He). Such a dataset consists

of laterally integrated depth dose profiles (Bragg curves), lateral dose profiles, as well as fragment spectra at different depths in water (H_2O)—the typical reference medium in radiotherapy—and is usually calculated with a suitable radiation transport code. Because nuclear fragmentation has a considerable impact on all of these data [15,16] the reaction cross section σ_R as a function of energy for $^4\text{He} + ^1\text{H}$ and $^4\text{He} + ^{16}\text{O}$ collisions needs to be accurately modeled in the transport code used for the calculation of ^4He basic data. At HIT the proton and ^{12}C ion basic data for the clinical treatment planning system have been calculated with the FLUKA Monte Carlo code [17–21], therefore FLUKA is also the natural choice for calculation of the basic data for future applications of ^4He ions. Within this scope, the performance of the code in calculating dose distributions in water generated by ^4He ions in the therapeutic energy range was recently evaluated by comparison of simulation results with extensive dosimetric measurements [12,13]. The overall agreement between the FLUKA predictions and the measured dose distributions was good. However, it was observed that especially at high ^4He energies FLUKA tended to over-estimate the dose at the Bragg peak by up to $\approx 6\%$ [13]. The cause for this discrepancy was investigated by comparing the FLUKA reaction cross section model with ^4He cross section measurements that we recently performed at HIT for the system $^4\text{He} + ^{12}\text{C}$ [22]. This comparison suggested that an underestimation of σ_R by the FLUKA model at intermediate energies (≈ 200 MeV/u) might be the cause for the overprediction of the Bragg peak dose in H_2O . This effect can be understood as follows: the dose deposited by nuclear fragments is more blurred than the dose from the primary ions which all stop around a certain depth and create the Bragg peak at this position. Consequently, the peak dose in calculated depth dose profiles gets overestimated if the reaction cross section is modeled too low because the number of primary ions that reach the Bragg peak depth without undergoing fragmentation is predicted too high.

We therefore decided to complement previous ^4He fragmentation studies related to radiotherapy [22–25] and to further support the nuclear reaction modeling for ^4He ions in FLUKA by extending our previous experiment to a broader set of target materials. Thin C, CH_2 , Si, SiO_2 , and H_2O targets were irradiated with ^4He ions in the intermediate energy range during this new measurement campaign at HIT. In this experiment charge- and mass-changing cross sections for the systems $^4\text{He} + ^1\text{H}$, $^4\text{He} + ^{12}\text{C}$, $^4\text{He} + ^{16}\text{O}$, and $^4\text{He} + ^{28}\text{Si}$ in the energy range 70–220 MeV/u were obtained. This article presents these new cross section data in comparison with

previous experimental data and with the widely used reaction cross section parametrization by Tripathi *et al.* [26,27]. In order to better match our measured cross sections, certain changes of the parameters within the Tripathi model for ^4He -nucleus collisions are suggested. These changes could be easily adopted in any existing implementation of this model.

II. METHODS AND MATERIALS

A. Experimental setup

The experimental setup used for the measurements is almost identical to the setup used in our previous experiment [22] and is based on the nuclear attenuation method using a ΔE - E scintillator telescope. A schematic drawing of the setup is shown in Fig. 1.

A pencil beam of ^4He ions impinged on a start scintillator (1 mm thick BC-400-like) which triggered the data acquisition. The ions then penetrated the target and were stopped within a ΔE - E scintillator telescope (5 mm thick BC-400-like and 14 cm long BaF_2 , both hexagonal with inner diameters of 10 cm and 8.5 cm, respectively).

Fragmentation reactions of the primary ^4He ions within the targets lead to combinations of a remarkably small number of fragment species, namely ^3He , ^3H , ^2H , ^1H , and neutrons. Also nucleon-pickup reactions lead only to unbound nuclei which immediately decay back into these species. Nuclear reactions that lead to no remaining He (^4He or ^3He) in the final state are referred to as charge-changing reactions (loss of at least one proton) whereas reactions without ^4He in the final state are called mass-changing reactions (loss of at least one nucleon).

The number of transmitted ^4He ions and ^3He fragments generated within the target could be determined by correlation of the signals from the ΔE scintillator with the signals from the BaF_2 scintillator. The larger angular coverage of the ΔE scintillator (81° to the beam axis) compared to the BaF_2 scintillator (72° to the beam axis) was exploited to ensure that only a negligible fraction of primary ions could be scattered out of the telescope's acceptance. This is important because full geometrical acceptance for the primary ions is required to measure total inelastic cross sections as presented here.

The slow synchrotron extraction was adjusted for a mean intensity of typically 1000 ions/s while the actual intensity fluctuated between 500 and 2000 ions/s. The measurements

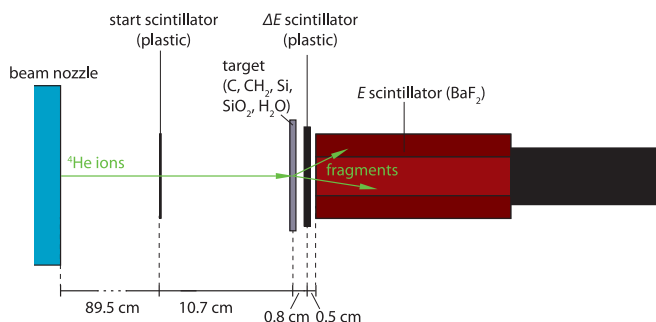


FIG. 1. Schematic of the experimental setup used at HIT to measure the charge- and mass-changing cross sections for ^4He ions impinging on different targets.

TABLE I. List of the targets used for ^4He cross section measurements.

Target material	Density (g/cm ³)	Thicknesses (cm)
C	1.83	0.5, 0.7, 1.0, 1.2
CH ₂	0.947	0.5, 1.0, 2.0
Si	2.33	0.4, 0.8, 1.6
SiO ₂	2.204	0.4, 0.8, 1.6
H ₂ O	1.0	2.22, 3.25 + flask ^a

^aCell culture flasks with 2×0.18 cm polystyrene walls.

were performed at three different primary energies (80, 130, and 220 MeV/u). Between 3×10^5 and 8×10^5 events were recorded for each energy and target thickness.

B. Targets

In Table I the different targets used for the ^4He cross section measurements are listed. For each ^4He energy used also a no-target measurement was performed to correct by the fragmentation occurring within the beam nozzle, the start scintillator, and the air gap. For most energy-material combinations at least two targets with different thicknesses were irradiated to have redundant information and to be able to check for robustness of the data analysis method.

By subtracting the cross sections measured on the elemental targets (C and Si) from those measured on the compound targets (CH₂ and SiO₂) the elemental cross section of the other element (H and O) can be calculated according to

$$\sigma^{\text{H}} = \frac{\sigma^{\text{CH}_2} - \sigma^{\text{C}}}{2}, \quad (1)$$

$$\sigma^{\text{O}} = \frac{\sigma^{\text{SiO}_2} - \sigma^{\text{Si}}}{2}. \quad (2)$$

For redundancy a measurement at a primary energy of 220 MeV/u using H₂O targets was also performed. For this purpose cell culture flasks (Corning 3073 and T-150) with two different thicknesses (2.22 cm and 3.25 cm + 2×0.18 cm polystyrene walls) were filled with water. To account for the fragmentation occurring within the walls of the flasks, an additional no-target measurement for each of the empty flasks was performed.

Carbon targets were already used during our previous experiment [22]. To check for consistency between the two experiments the carbon data point for the highest ^4He energy (220 MeV/u) was measured again. Additionally one new C data point at 80 MeV/u primary energy was measured in the present campaign to further extend the energy range explored in our previous experiment.

C. Alignment and beam spot characterization with CMOS sensor

To align the experimental setup as precisely as possible position, size and shape of the beam spot at low intensity were determined in advance with a set of MIMOSA28 CMOS sensors with high spatial resolution [28]. Figure 2 shows the measured beam spot profiles for the three ^4He energies used.

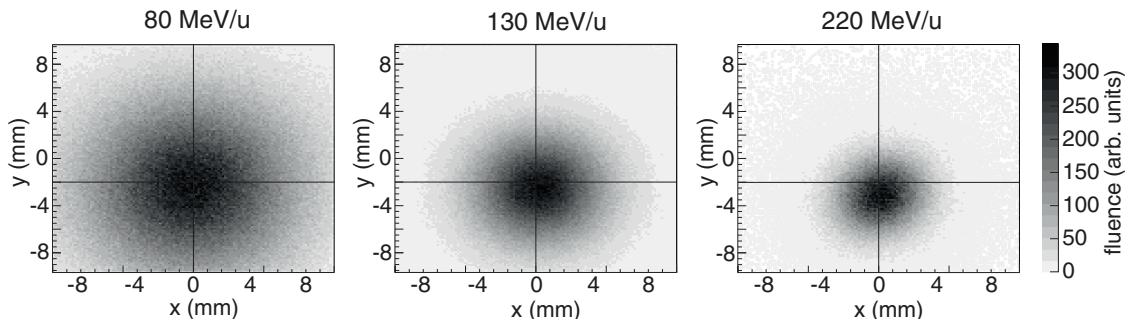


FIG. 2. Beam spots at low intensity measured with the CMOS sensor at the isocenter for the three ^4He energies used. The coordinate system corresponds to the positioning lasers in the experimental room and the lines mark the center of the aligned scintillator telescope.

The beam spot gets broader towards lower energies due to the increased lateral scattering within the beam nozzle (≈ 2 mm water equivalent thickness). A vertical shift relative to the isocenter (marked by positioning lasers in the experimental room) can be observed for all three energies. Based on these CMOS measurements the scintillator telescope was aligned with a vertical shift of 2 mm relative to the positioning lasers.

For the highest energy (220 MeV/u) there was still a shift of ≈ 1 mm left in the final alignment. However, for comparison, the inner diameter of the BaF_2 scintillator (85 mm) is large against this shift and against the sizes of the beam spots. Thus the scintillator telescope had practically full acceptance for the primary ^4He ions at all energies used.

D. Data acquisition

The scintillator pulses (start, ΔE , and E) were acquired with a Tektronix DSA 72004C fast sampling oscilloscope at a sample rate of 3.1 GS/s in event-by-event mode. The sampling of the pulses as waveforms provided a lot of additional information (pulse shape, time over threshold, double hit detection) compared to standard experimental electronics (e.g., analog-to-digital converters and charge-to-digital converters) which justifies the higher amount of stored data.

From these waveforms several characteristic quantities are calculated, e.g., integral, peak, ratio of integral to peak (further referred to as *pulse shape*), and time over threshold. Especially the pulse shape of the E scintillator (consisting of BaF_2) is crucial for the present analysis method because it provides an excellent separation of ions with different atomic numbers (e.g., primary He ions and their H fragments) [29].

III. DATA ANALYSIS

The data analysis and the particle identification were performed using the ROOT framework [30]. This procedure was almost completely automatized by ROOT scripts developed for the previous experiment. A detailed description can be found in the corresponding publication [22] while in the following only a short summary of the method is given.

In the first analysis step the valid events are selected on the basis of the following criteria on the start scintillator to exclude beam contaminants and double hits. Only events where the peak height and the integral of the pulse of the

start scintillator calculated from the waveform lay within ± 2.5 standard deviations from the corresponding average value were taken as valid events. Furthermore, events where the start scintillator's time over threshold was considerably larger than average were also excluded. By analyzing the time of arrival of the remaining events (typically more than 95% of the recorded events) it could be ensured that the temporal distance between consecutive events was larger than the long decay time component of the BaF_2 scintillator ($\tau = 630$ ns).

Figure 3 shows examples of ΔE -pulse-shape and ΔE spectra for 130 MeV/u ^4He ions with no target and after traversing a 16 mm Si target, according to which the data analysis method is explained in the following. The separation thresholds $T1$ and $T2$ (see Fig. 3) are the only analysis parameters that have to be set by hand. The correlation of the ΔE signals generated in the 5 mm plastic scintillator with the pulse shape of the BaF_2 scintillator allows a clear identification of the major fraction of the He ions leaving the target [upper right quadrant in Figs. 3(a) and 3(b)]. They are made up of the transmitted ^4He ions as well as the ^3He fragments produced in the target. A small part of the He events (10–20% depending on the energy) overlap with the H fragment events in the ΔE -pulse-shape plots (upper left quadrant in Figs. 3(a) and 3(b)) due to fragmentation reactions in the thick BaF_2 scintillator. The number of these events is estimated from the ΔE spectrum of the overlap region, assuming that the shape of the He ΔE spectrum is the same as in the non-overlap region. This is well justified by the assumption that a nuclear reaction of an ion within the BaF_2 , which causes the overlap, occurs independently of its prior energy deposition within the ΔE scintillator. The number of He events after the target gives information about the charge-changing cross section, while for determination of the mass-changing cross section they additionally need to be separated into primary ^4He ions and ^3He fragments. This is achieved through a fit on the ΔE spectrum of the identified He events. The ΔE spectrum can be well fitted by the sum of a Gauss distribution and one or two Landau distributions [Figs. 3(c) and 3(d)]. For the measurements with targets the ^4He events are represented by the Gauss fraction because their energy spectrum (and thus their ΔE spectrum) is still relatively sharp. The ^3He events are represented by the Landau fraction because the energy spectrum of the fragments is much broader and some ^3He events show a neutron coincidence [creating the small peak

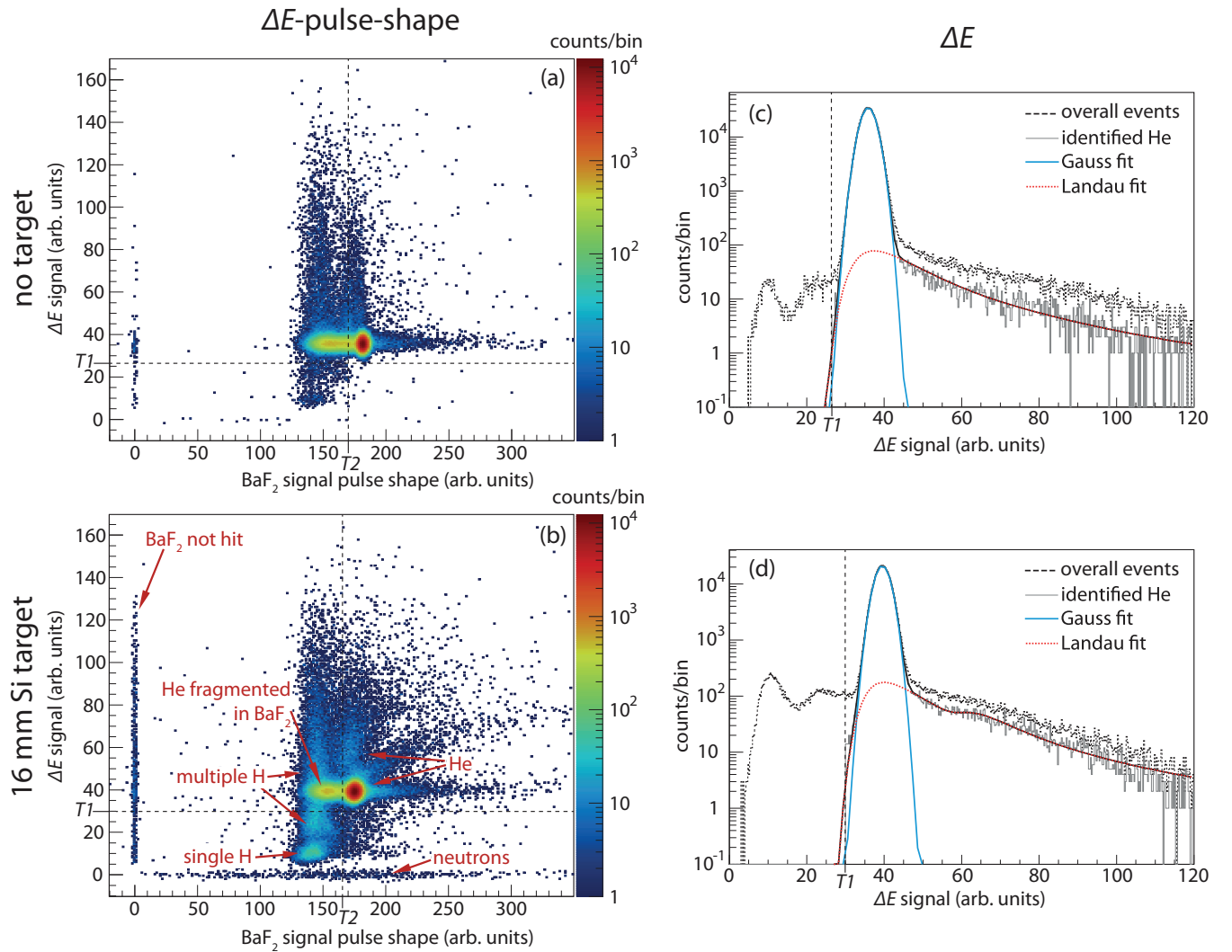


FIG. 3. Examples of ΔE -pulse-shape spectra (left panels) and ΔE spectra (right panels) for 130 MeV/u ^4He ions with no target (upper panels) and after traversing 16 mm of Si (lower panels). The term ΔE signal stands for the integral of the waveform of the ΔE scintillator, and BaF_2 signal pulse shape stands for the ratio of integral to peak calculated from the signal of the start scintillator. Double hits are already excluded by applying appropriate selection criteria on the signal of the start scintillator (see text). The thresholds T_1 and T_2 have been set by hand to separate the He events in the upper right corner of the ΔE -pulse-shape plots from their H fragments. The origin of the event clusters visible in the spectra for 16 mm Si is indicated by the arrows. A detailed description is given in the text.

right to the main peak in the Landau fraction in Fig. 3(d). The small contribution of the primary ^4He ions to the Landau tail is determined in a no-target run [Fig. 3(c)] considering that the primary beam is only negligibly contaminated by ^3He fragments. The Landau contribution in the no-target run is then subtracted from the Landau fraction obtained in the measurements with target [Fig. 3(d)].

Finally the relative number of He or ^4He ions as a function of target thickness z (referred to as *attenuation curve*), can be fitted with a function according to

$$\frac{N}{N_0} = A_0 e^{-z \frac{n}{V} \sigma}, \quad (3)$$

where n/V is the number of targets (nuclei or molecules) per volume, A_0 a value for fine-tuning the fit (varies not more than few permille around 1), and σ the cross section for the

observed reaction ($\sigma_{\Delta Z}$ for He ions as a function of z and $\sigma_{\Delta A}$ for ^4He ions as a function of z).

A. Uncertainty estimation

There are different uncertainties to be considered for the presented cross section measurements. The uncertainty estimation method for the cross sections obtained from single targets is the same as that described in our previous work [22] and considers the statistical component originating from the finite amount of measured events as well as systematic components introduced by the application of fit methods and extrapolations into overlap regions in the measured spectra.

The uncertainties of the two single target cross sections (σ^{C} and σ^{CH_2} or σ^{Si} and σ^{SiO_2}) propagate both into the uncertainty of the calculated elemental cross sections (σ^{H} or σ^{O}). This is

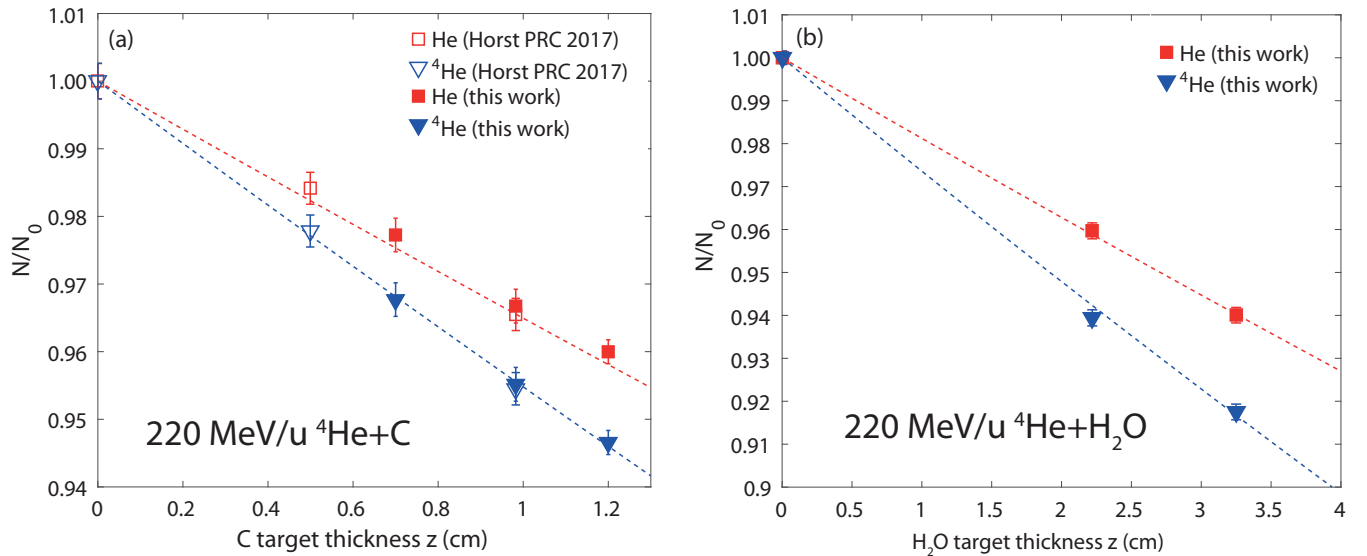


FIG. 4. Examples of attenuation curves measured for C (a) and H_2O (b) targets for 220 MeV/u ^4He ions. The dashed lines represent the corresponding fit functions according to Eq. (3) to extract the charge- and mass-changing cross sections from the attenuation curves. In panel (a) the measured attenuation values for C targets from our previous experiment [22] are shown for comparison. The plotted fit functions for the C targets were not recalculated with the attenuation values measured in the new campaign; however, they agree with all new values within the error bars. The C curves are normalized to the no-target measurement, while the H_2O curves are normalized to the measurements behind the empty flasks (see text).

taken into account by calculating the square root of the sum of the squared uncertainties from the single measurements, considering that they are uncorrelated.

The energy loss of the primary ^4He ions within the targets smeared the energy at which the measured reactions took place. This effect is considered by simulating the primary ion transport through the different targets using FLUKA. The measured cross sections are given for the energy at the center of the thickest target used with an uncertainty interval covering the energy loss before and after the target center.

IV. RESULTS AND DISCUSSION

Two examples of nuclear attenuation curves (for C and H_2O targets) obtained by analysis of the recorded ΔE -pulse-shape spectra behind different target thicknesses are shown in Fig. 4. The number of transmitted He and ^4He ions are normalized to the number obtained in the no-target measurement (attenuation in C) or in the measurement behind the empty flasks (attenuation in H_2O), respectively. The agreement of the measured data behind the C targets with our previous measurements and fit functions proves the consistency of the two experiments. The charge- and mass-changing cross sections for each energy-target combination could be extracted from the measured attenuation curves by exponential fits. The fit functions look almost linear because the thicknesses of the targets used were small against the mean free path of the ions.

The measured charge- and mass-changing cross sections for C, CH_2 , Si, SiO_2 , and H_2O targets as well as the calculated cross sections for H and O targets are listed in Table II. The (inclusive) ^3He production cross section can be calculated by subtracting $\sigma_{\Delta Z}$ from $\sigma_{\Delta A}$ because fragmentation into ^3He

is the only mass-changing but non-charge-changing reaction channel that can occur for ^4He projectiles.

In Fig. 5 the mass-changing cross sections for the elemental targets C, O, Si, and H as a function of kinetic energy obtained at the present experiment are shown together with the available data from the literature (C targets [31–37], O targets [31,32,37], Si targets [31,32,38], H targets [35,39–41]). The shown reference data include also a few charge-changing cross sections which are slightly lower than the corresponding mass-changing cross sections because the contribution of neutron-removal reactions is missing. For comparison the reaction cross section parametrizations by Tripathi *et al.* for ^4He -nucleus [26] [panels (a)–(c)] and for ^4He - ^1H collisions [27] [panel (d)] are plotted. The target nuclei are labeled by their main isotope. This is done for simplicity, while in the analysis the natural isotopic composition of the targets was taken into account.

The measured mass-changing cross sections presented here are in good agreement with the reference data from the literature. At the lower end of the investigated energy range (70 MeV/u) is a rather smooth transition from the present cross sections to the experimental data by Ingemarsson *et al.* [32] [^4He -nucleus systems, panels (a)–(c)] and Sourkes *et al.* [39] [^4He - ^1H system, panel (d)]. The charge-changing cross sections at high energies reported by Ferrando *et al.* [36] and Webber *et al.* [37] (measured in inverse kinematics, by irradiating a ^4He target with ^{12}C and ^{16}O beams) compare well with the ^4He charge-changing cross sections listed in Table II and those from our previous experiment [22]. The relative uncertainties of the H and O cross sections are considerably larger than those of the C and Si targets due to the propagation of the compound target cross section uncertainties into the errors of the calculated elemental cross sections. However, the

TABLE II. Measured mass- and charge-changing cross sections for ^4He ions with different energies on different targets. The upper values were directly measured and the values for H and O were calculated from the upper values together with our previous dataset for C targets [22] according to Eqs. (1) and (2).

Target	Method	Kinetic energy (MeV/u)	Charge-changing cross section $\sigma_{\Delta Z}$ (mb)	Mass-changing cross section $\sigma_{\Delta A}$ (mb)
C	measured	74 ± 4	277 ± 33	602 ± 66
CH ₂	measured	71 ± 8	321 ± 47	875 ± 103
CH ₂	measured	119 ± 10	442 ± 22	731 ± 51
CH ₂	measured	215 ± 5	490 ± 23	729 ± 47
Si	measured	71 ± 8	304 ± 44	961 ± 110
Si	measured	119 ± 10	487 ± 26	816 ± 59
Si	measured	213 ± 7	620 ± 26	792 ± 43
SiO ₂	measured	71 ± 8	806 ± 99	2317 ± 251
SiO ₂	measured	119 ± 10	1240 ± 58	2042 ± 139
SiO ₂	measured	213 ± 7	1563 ± 58	1959 ± 98
H ₂ O	measured	213 ± 7	568 ± 35	800 ± 58
H	calculated	71 ± 8	22^{+57}_{-22}	137 ± 69
H	calculated	119 ± 10	60 ± 31	117 ± 37
H	calculated	215 ± 5	49 ± 30	104 ± 35
O	calculated	71 ± 8	251 ± 108	678 ± 152
O	calculated	119 ± 10	377 ± 63	613 ± 88
O	calculated	213 ± 7	472 ± 64	584 ± 75

reasonable accordance of the measured data with the literature data suggests that this approach provides a rather conservative estimate of the actual measurement uncertainty.

The total reaction cross section σ_R for proton-nucleus and nucleus-nucleus systems follows the trend of the nucleon-nucleon total cross section as a function of energy due to the microscopic nature of these collisions [2,33,42]. The reaction cross section shows a maximum at a few 10 MeV/u and then drops down to a minimum lying at a few 100 MeV/u. As the pion production channels open, σ_R rises again slightly before it finally stays constant towards higher energies. This general behavior of σ_R is visible in the plotted experimental cross sections for ^4He -induced reactions and is well reflected by the parametrizations.

For the ^4He -nucleus reactions ($^4\text{He} + ^{12}\text{C}$, $^4\text{He} + ^{16}\text{O}$, and $^4\text{He} + ^{28}\text{Si}$) also a modified version of the Tripathi model based on our new cross section data is shown in Fig. 5. In the original Tripathi model [26] the parameter D which modifies the ^4He -nucleus reaction cross section at low and intermediate energies is calculated according to

$$D_{\text{Tripathi}} = 2.77 - 8.0 \times 10^{-3} \times A_T + 1.8 \times 10^{-5} \times A_T^2 - \frac{0.8}{1 + e^{\left(\frac{250-E}{75}\right)}}, \quad (4)$$

where A_T is the mass number of the target nucleus and E is the kinetic energy in MeV/u. Tripathi *et al.* optimized the parameter D in their model to match the experimental data by Auce *et al.* [31] and Jaros *et al.* [35]. However, the data by Auce *et al.* were later measured again by Ingemarsson *et al.* [32], using an improved version of the experimental setup developed for the Auce experiment. These revised cross sections are slightly higher than the old values that Tripathi *et al.* used for their model optimization, consequently the model should be updated to match the Ingemarsson data.

The experimental cross sections presented in this work suggest that the Tripathi reaction cross section parametrization should also be increased to higher values in the energy range 70–220 MeV/u. Therefore we suggest to modify the parameter D according to

$$D_{\text{Tripathi}}^{\text{optimized}} = 2.2 - 8.0 \times 10^{-3} \times A_T + 1.8 \times 10^{-5} \times A_T^2 - \frac{0.3}{1 + e^{\left(\frac{120-E}{50}\right)}}. \quad (5)$$

As shown in Fig. 5 our optimized version of the Tripathi model [solid line in panels (a)–(c)] matches the experimental cross sections presented in this work and in our previous article and those by Ingemarsson *et al.* better than the original model, while the prediction for high energies (>1 GeV/u) is almost unaffected by the proposed parameter changes. Besides the agreement with the new experimental data, our modified parametrization is also in good accordance with the theoretical $^4\text{He} + ^{12}\text{C}$ reaction cross section prediction from optical model calculations by DeVries and Peng [2]. Using the optimized Tripathi reaction cross section model instead of the original one is expected to result in considerable improvements of ^4He ion transport calculations related to radiotherapy applications (e.g., calculation of dose distributions in a patient) because C and O are the main constituents of biological soft tissues. The optimized model still underestimates the Ingemarsson data points for the $^4\text{He} + ^{28}\text{Si}$ system at low energy. However, it is in agreement with the data by Warner *et al.* [38]. The overall agreement of the modified version with the experimental data is better than for the original model and at intermediate energies the scaling towards heavier target nuclei (up to ^{28}Si) still works well.

As an alternative to our modified Tripathi model, the reaction cross section model by Shen *et al.* [43] (improved by Sihver *et al.* [44]) may be used. Its predictions of ^4He -nucleus

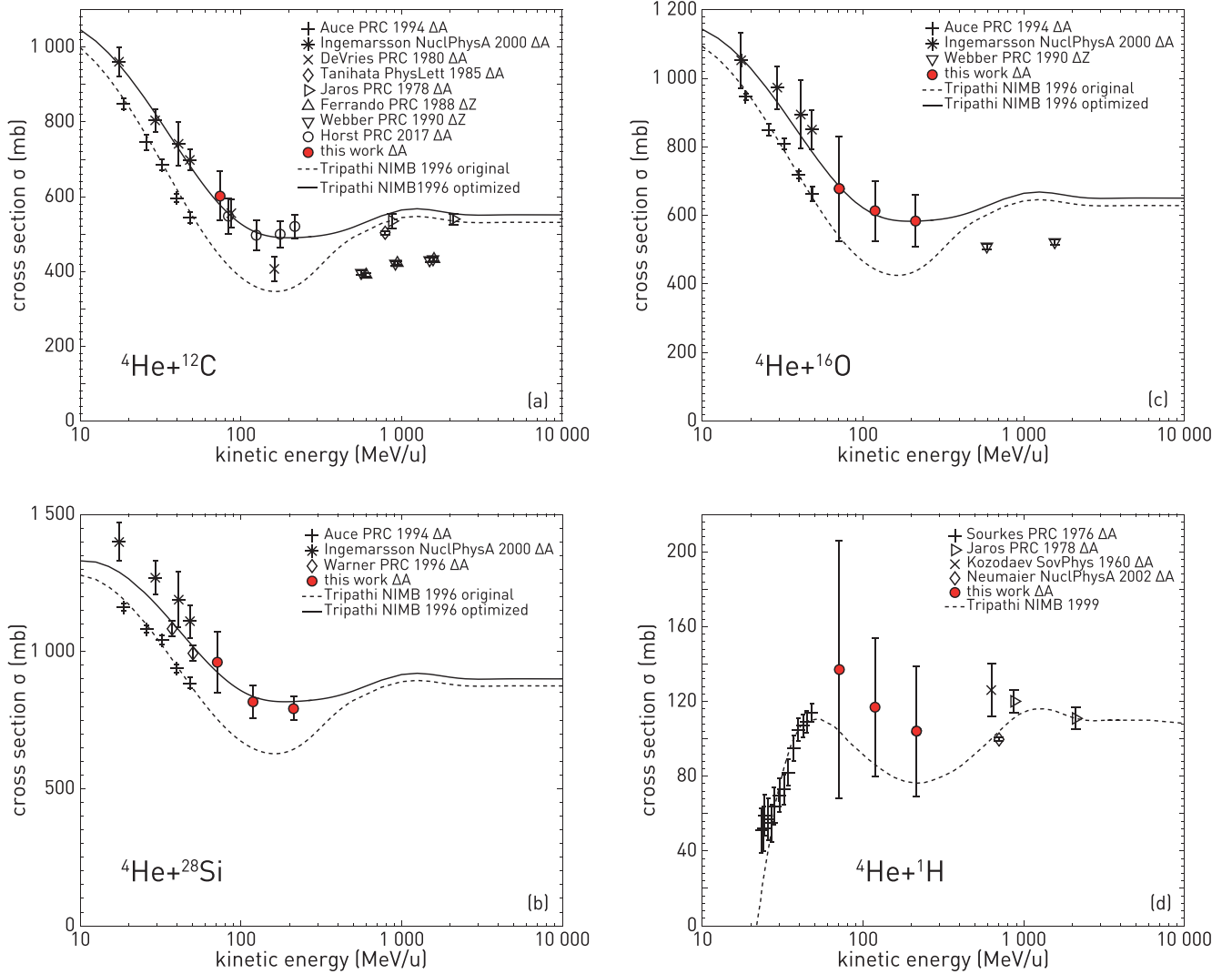


FIG. 5. Measured mass-changing cross sections $\sigma_{\Delta\Delta}$ for ^4He ions on different elemental targets (C, O, Si and H) compared with reference data from the literature ($\sigma_{\Delta\Delta}$ and $\sigma_{\Delta Z}$) [31–41]. For the ^4He -nucleus systems ($^4\text{He} + ^{12}\text{C}$, $^4\text{He} + ^{16}\text{O}$, $^4\text{He} + ^{28}\text{Si}$) the Tripathi parametrization for heavy ion collisions [26] as well as a version optimized on basis of the new measured cross sections are shown. For the $^4\text{He} + ^1\text{H}$ system the prediction of the Tripathi parametrization for light systems [27] is plotted.

reaction cross sections are also in reasonable agreement with our experimental data and those by Ingemarsson for C and O targets. The Shen model is available as an option in some Monte Carlo codes, e.g. GEANT4 [45] which was used by Fuchs *et al.* [46] and Knäusl *et al.* [47] to study possible radiotherapy applications of ^4He ions.

It should be pointed out that neither the mass-changing cross sections from this work nor the experimental data that are shown for comparison account for inelastic scatter reactions where the target nucleus gets excited or fragments but the projectile stays intact. For most colliding systems this component is negligible, but for the extraordinary stable ^4He nucleus (first excited state at ≈ 20 MeV, no bound excited state) a non-negligible contribution to the total reaction cross section can be assumed. A contribution of ≈ 5 –15% (depending on the energy and the target nucleus) has been predicted by optical model calculations [48], which is in the same order as the prediction by the event generators implemented

in FLUKA. Therefore the inelastic scatter component should be considered separately for radiation transport codes that take into account excitation or fragmentation of target nuclei (particularly Monte Carlo transport codes) and subtracted from the modeled total reaction cross section σ_R to compare it to the experimental mass-changing cross sections $\sigma_{\Delta\Delta}$. For deterministic one-dimensional transport codes like HZETRN [49] or TRIP98 [3,14] which consider only projectile fragmentation it is sufficient to model only $\sigma_{\Delta\Delta}$ as an estimate of σ_R .

For the $^4\text{He} + ^1\text{H}$ reaction cross section model [solid line in Fig. 5(d)], also designed by Tripathi *et al.* [27], we suggest no parameter changes because its prediction matches our measured values within the error bars, which are relatively large due to the propagation of the C and CH_2 cross section errors into the error of the H cross section. With more complex measurement methods (e.g., by using a liquid hydrogen target instead of a combination of C and CH_2 targets) there might still be room for improvements. However, it should be noted

TABLE III. ^4He charge- and mass-changing cross sections measured on H_2O targets compared with those calculated from the H and O cross sections obtained from the C, CH_2 , Si, and SiO_2 target measurements (see text). For further comparison, the mass-changing cross section estimated by Rovituso *et al.* [25] from a thick target measurement is shown.

Method	Kinetic energy (MeV/u)	Charge-changing cross section $\sigma_{\Delta Z}$ (mb)	Mass-changing cross section $\sigma_{\Delta A}$ (mb)
measured (this work)	213 ± 7	568 ± 35	800 ± 58
calculated (this work)	213 ± 7	569 ± 70	792 ± 83
measured [25]	200		636 ± 76

that the major contributor to the reaction cross section of H_2O (the reference medium in radiotherapy) is the O nucleus rather than the two H nuclei.

In Table III the charge- and mass-changing cross sections obtained for 213 MeV/u ^4He ions on H_2O targets by calculation (summation of the H and O cross sections obtained from measurements on C, CH_2 , Si, and SiO_2) and by a direct measurement (using the H_2O filled flasks) are compared.

They are in good agreement with each other, which proves the self-consistency of the presented dataset. The *total fragmentation cross section* (equivalent to our definition of the mass-changing cross section) estimated by Rovituso *et al.* [25] from a thick target measurement is considerably lower than the values presented in this work. Most probably, this discrepancy can be explained by comparing the methods applied for particle identification. The standard ΔE - E method used by Rovituso *et al.* has large overlap areas in the spectra used for identification while in the present work an improved and more robust, particle identification method is used, which exploits the pulse shape of the BaF_2 scintillator as an additional measure for the atomic number of the outgoing ions. Also cross section measurements with thin targets are superior over thick target measurements concerning the required full acceptance. Furthermore the obtained elemental cross sections shown in Fig. 5 are fully consistent with the literature data and clearly follow the expected trend.

V. CONCLUSION

Measurements of charge- and mass-changing cross sections for the systems $^4\text{He} + ^{12}\text{C}$, $^4\text{He} + ^{16}\text{O}$, $^4\text{He} + ^{28}\text{Si}$, and $^4\text{He} + ^1\text{H}$ in the energy range 70–220 MeV/u were performed. These data are relevant for future radiotherapy applications of ^4He ion beams as planned at the Heidelberg Ion-Beam Therapy Center (HIT). The presented cross sections can be useful for the validation and optimization of ^4He nuclear reaction models used in heavy ion transport codes. The Tripathi parametrization of the nuclear reaction cross section σ_R [26], which is implemented in many Monte Carlo or other types of radiation transport codes, was compared to the new experimental data. The comparison showed that the model underpredicts the ^4He -nucleus reaction cross section at intermediate energies. Therefore parameter changes that lead to a better fit to the experimental cross sections were proposed. This optimization can easily be adopted in heavy ion transport

codes that use the Tripathi model and will improve their predictive power, in particular for applications related to ^4He ion therapy, e.g., the calculation of dose distributions or fragment distributions within a patient.

The presented cross sections will also be used to improve the accuracy of the nuclear reaction cross section model for ^4He ions implemented in FLUKA. Therefore, this work will have a direct clinical impact, as FLUKA is used to generate the basic input data for the treatment planning system at HIT. The adjustment of the FLUKA parametrizations and the effects on dose calculation will be the subject of future work.

Another research field that might benefit from the novel cross section data presented in this article is space radiation protection [50,51]. ^4He ions make up $\approx 10\%$ of the primary galactic cosmic radiation, with an energy spectrum peaking at intermediate energies. Nuclear fragmentation of the primary ions, e.g., within the structures of a spacecraft, has to be taken into account for the shielding design, and therefore accurate ^4He transport models are required also in this field [48].

In the future, the present study on total cross sections for ^4He -induced reactions could be extended towards higher energies because the energy range 200–800 MeV/u is still almost unexplored. The measurement uncertainty of $^4\text{He} + ^1\text{H}$ reaction cross sections could be improved by increasing the experimental effort, and the gap in the energy range 50–600 MeV/u could be filled. The investigation of heavier target materials could be an option to better understand the underlying scaling laws and systematics. Future experiments could also focus on the measurement of partial cross sections for production of the individual fragment species (^3He , ^3H , ^2H , ^1H , and neutrons) as well as their angular distributions and energy spectra (double-differential yields) to further improve the nuclear reaction models and thereby the biological treatment planning for ^4He ions.

ACKNOWLEDGMENTS

The authors would like to thank the HIT accelerator team for providing the excellent ^4He beams. Furthermore the GSI target laboratory is acknowledged for its support concerning the targets. G.A. wants to thank the European Union's Horizon 2020 research and innovation program under the Marie Skłodowska-Curie Grant Agreement No. 675265 Optimization of Medical Accelerators (OMA) for funding.

- [1] S. Kox, A. Gamp, C. Perrin, J. Arvieux, R. Bertholet, J. F. Bruandet, M. Buenerd, R. Cherkaoui, A. J. Cole, Y. El-Masri, N. Longequeue, J. Menet, F. Merchez, and J. B. Viano, Trends of total reaction cross sections for heavy ion collisions in the intermediate energy range, *Phys. Rev. C* **35**, 1678 (1987).
- [2] R. M. DeVries and J. C. Peng, Nucleus-nucleus total reaction cross sections, *Phys. Rev. C* **22**, 1055 (1980).
- [3] M. Krämer, E. Scifoni, C. Schuy, M. Rovituso, W. Tinganelli, A. Maier, R. Kaderka, W. Kraft-Weyrather, S. Brons, T. Tessonier, K. Parodi, and M. Durante, Helium ions for radiotherapy? Physical and biological verifications of a novel treatment modality, *Med. Phys.* **43**, 1995 (2016).
- [4] D. Schardt, T. Elsässer, and D. Schulz-Ertner, Heavy-ion tumor therapy: Physical and radiobiological benefits, *Rev. Mod. Phys.* **82**, 383 (2010).
- [5] R. Grün, T. Friedrich, M. Krämer, K. Zink, M. Durante, R. Engenhart-Cabillic, and M. Scholz, Assessment of potential advantages of relevant ions for particle therapy: A model based study, *Med. Phys.* **42**, 1037 (2016).
- [6] A. Mairani, I. Dokic, G. Magro, T. Tessonier, F. Kamp, D. J. Carlson, M. Ciocca, F. Cerutti, P. R. Sala, A. Ferrari, T. T. Böhlen, O. Jäkel, K. Parodi, J. Debus, A. Abdollahi, and T. Haberer, Biologically optimized helium ion plans: Calculation approach and its in vitro validation, *Phys. Med. Biol.* **61**, 4283 (2016).
- [7] T. Tessonier, A. Mairani, W. Chen, P. Sala, F. Cerutti, A. Ferrari, T. Haberer, J. Debus, and K. Parodi, Proton and helium ion radiotherapy for meningioma tumors: A Monte Carlo-based treatment planning comparison, *Radiat. Oncol.* **13** (2018).
- [8] W. Saunders, J. R. Castro, G. T. Y. Chen, J. M. Collier, S. R. Zink, S. Pitluck, D. Char, P. Gutin, G. Gauger, C. A. Tobias, and E. L. Alpen, Helium-ion radiation therapy at the Lawrence Berkeley laboratory: Recent results of a northern California oncology group clinical trial, *Radiat. Res.* **104**, S227 (1985).
- [9] B. A. Ludewigt, W. T. Chu, M. H. Phillips, and T. R. Renner, Accelerated helium-ion beams for radiotherapy and stereotactic radiosurgery, *Med. Phys.* **18**, 36 (1991).
- [10] T. Haberer, J. Debus, H. Eickhoff, O. Jäkel, D. Schulz-Ertner, and U. Weber, The Heidelberg ion therapy center, *Radiother. Oncol.* **73**, S186 (2004).
- [11] T. Tessonier, A. Mairani, S. Brons, T. Haberer, J. Debus, and K. Parodi, Experimental dosimetric comparison of ^1H , ^4He , ^{12}C and ^{16}O scanned ion beams, *Phys. Med. Biol.* **62**, 3958 (2017).
- [12] T. Tessonier, T. T. Böhlen, F. Cerutti, A. Ferrari, P. Sala, S. Brons, T. Haberer, J. Debus, K. Parodi, and A. Mairani, Dosimetric verification in water of a Monte Carlo treatment planning tool for proton, helium, carbon and oxygen ion beams at the Heidelberg ion beam therapy center, *Phys. Med. Biol.* **62**, 6579 (2017).
- [13] T. Tessonier, A. Mairani, S. Brons, P. Sala, F. Cerutti, A. Ferrari, T. Haberer, J. Debus, and K. Parodi, Helium ions at the heidelberg ion beam therapy center: Comparisons between FLUKA Monte Carlo code predictions and dosimetric measurements, *Phys. Med. Biol.* **62**, 6784 (2017).
- [14] M. Krämer, O. Jäkel, T. Haberer, G. Kraft, D. Schardt, and U. Weber, Treatment planning for heavy-ion radiotherapy: Physical beam model and dose optimization, *Phys. Med. Biol.* **45**, 3299 (2000).
- [15] A. Lühr, D. C. Hansen, R. Teiwes, N. Sobolevsky, O. Jäkel, and N. Bassler, The impact of modeling nuclear fragmentation on delivered dose and radiobiology in ion therapy, *Phys. Med. Biol.* **57**, 5169 (2012).
- [16] M. Durante and H. Paganetti, Nuclear physics in particle therapy: A review, *Rep. Prog. Phys.* **79**, 096702 (2016).
- [17] A. Ferrari, P. R. Sala, A. Fassò, and J. Ranft, FLUKA: a multi-particle transport code, CERN Report No. CERN-2005-10, 2005.
- [18] T. T. Böhlen, F. Cerutti, M. P. W. Chin, A. Fassò, A. Ferrari, P. G. Ortega, A. Mairani, P. R. Sala, G. Smirnov, and V. Vlachoudis, The FLUKA code: Developments and challenges for high energy and medical applications, *Nucl. Data Sheets* **120**, 211 (2014).
- [19] G. Battistoni, J. Bauer, T. T. Böhlen, F. Cerutti, M. P. W. Chin, R. Dos Santos Augusto, A. Ferrari, P. G. Ortega, W. Kozłowska, G. Magro, A. Mairani, K. Parodi, P. R. Sala, P. Schoofs, T. Tessonier, and V. Vlachoudis, The FLUKA code: An accurate simulation tool for particle therapy, *Front. Oncol.* **6** (2016).
- [20] G. Battistoni, T. Boehlen, F. Cerutti, P. W. Chin, L. S. Esposito, A. Fassò, A. Ferrari, A. Lechner, A. Empl, A. Mairani, A. Mereghetti, P. Garcia Ortega, J. Ranft, S. Roesler, P. R. Sala, V. Vlachoudis, and G. Smirnov, Overview of the FLUKA code, *Ann. Nucl. Energy* **82**, 10 (2015).
- [21] K. Parodi, A. Mairani, S. Brons, B. G. Hasch, F. Sommerer, J. Naumann, O. Jäkel, T. Haberer, and J. Debus, Monte Carlo simulations to support start-up and treatment planning of scanned proton and carbon ion therapy at a synchrotron-based facility, *Phys. Med. Biol.* **57**, 3759 (2012).
- [22] F. Horst, C. Schuy, U. Weber, K.-T. Brinkmann, and K. Zink, Measurement of charge- and mass-changing cross sections for $^4\text{He} + ^{12}\text{C}$ collisions in the energy range 80–220 MeV/u for applications in ion beam therapy, *Phys. Rev. C* **96**, 024624 (2017).
- [23] G. Aricò, T. Gehrke, J. Jakubek, R. Gallas, S. Berke, O. Jäkel, A. Mairani, A. Ferrari, and M. Martisiková, Investigation of mixed ion fields in the forward direction for 220.5 MeV/u helium ion beams: Comparison between water and PMMA targets, *Phys. Med. Biol.* **62**, 8003 (2017).
- [24] M. Marafini, R. Paramatti, D. Pinci, G. Battistoni, F. Collamati, E. De Lucia, R. Faccini, P. M. Frallicciardi, C. Mancini-Terracciano, I. Mattei, S. Muraro, L. Piersanti, M. Rovituso, A. Rucinski, A. Russomando, A. Sarti, A. Sciuabba, E. Solfaroli Camillocci, M. Toppi, G. Traini, C. Voena, and V. Patera, Secondary radiation measurements for particle therapy applications: Nuclear fragmentation produced by ^4He ion beams in a PMMA target, *Phys. Med. Biol.* **62**, 1291 (2017).
- [25] M. Rovituso, C. Schuy, U. Weber, S. Brons, M. A. Cortés-Giraldo, C. La Tessa, E. Piasetzky, D. Israeli, D. Schardt, M. Toppi, E. Scifoni, M. Krämer, and M. Durante, Fragmentation of 120 and 200 MeV u^{-1} ^4He ions in water and PMMA targets, *Phys. Med. Biol.* **62**, 1310 (2017).
- [26] R. K. Tripathi, F. A. Cucinotta, and J. W. Wilson, Accurate universal parameterization of absorption cross sections, *Nucl. Instrum. Methods Phys. Res. B* **117**, 347 (1996).
- [27] R. K. Tripathi, F. A. Cucinotta, and J. W. Wilson, Accurate universal parameterization of absorption cross sections III – light systems, *Nucl. Instrum. Methods Phys. Res. B* **155**, 349 (1999).
- [28] I. Valin *et al.*, A reticle size CMOS pixel sensor dedicated to the STAR HFT, *J. Instrum.* **7**, C01102 (2012).

- [29] R. Novotny, The BaF₂ spectrometer TAPS: A system for high energy photon and neutral meson detection, *Nucl. Tracks Radiat. Meas.* **21**, 23 (1993).
- [30] R. Brun and F. Rademakers, ROOT – An object oriented data analysis framework, *Nucl. Instrum. Methods Phys. Res. A* **389**, 81 (1997).
- [31] A. Auce, R. F. Carlson, A. J. Cox, A. Ingemarsson, R. Johansson, P. U. Renberg, O. Sundberg, G. Tibell, and R. Zorro, Reaction cross sections for 75–190 MeV alpha particles on targets from ^{12}C to ^{208}Pb , *Phys. Rev. C* **50**, 871 (1994).
- [32] A. Ingemarsson, J. Nyberg, P. U. Renberg, O. Sundberg, R. F. Carlson, A. J. Cox, A. Auce, R. Johansson, G. Tibelli, D. T. Khoa, and R. E. Warner, New results for reaction cross sections of intermediate energy α -particles on targets from ^9Be to ^{208}Pb , *Nucl. Phys. A* **676**, 3 (2000).
- [33] R. M. DeVries, N. J. DiGiacomo, J. S. Kapustinsky, J. C. Peng, W. E. Sondheim, J. W. Sunier, J. G. Cramer, R. E. Loveman, C. R. Gruhn, and H. H. Wieman, Dominance of nucleon-nucleon interactions in $\alpha + ^{12}\text{C}$ total reaction cross sections, *Phys. Rev. C* **26**, 301 (1982).
- [34] I. Tanihata, H. Hamagaki, O. Hashimoto, S. Nagamiya, Y. Shida, N. Yoshikawa, O. Yamakawa, K. Sugimoto, T. Kobayashi, D. E. Greiner, N. Takahashi, and Y. Nojiri, Measurements of interaction cross sections and radii of He isotopes, *Phys. Lett. B* **160**, 380 (1985).
- [35] J. Jaros, A. Wagner, L. Anderson, O. Chamberlain, R. Z. Fuzesy, J. Gallup, W. Gorn, L. Schroeder, S. Shannon, G. Shapiro, and H. Steiner, Nucleus-nucleus total cross sections for light nuclei at 1.55 and 2.89 GeV/c per nucleon, *Phys. Rev. C* **18**, 2273 (1978).
- [36] P. Ferrando, W. R. Webber, P. Goret, J. C. Kish, D. A. Schrier, A. Soutoul, and O. Testard, Measurement of ^{12}C , ^{16}O , and ^{56}Fe charge changing cross sections in helium at high energy, comparison with cross sections in hydrogen, and application to cosmic-ray propagation, *Phys. Rev. C* **37**, 1490 (1988).
- [37] W. R. Webber, J. C. Kish, and D. A. Schrier, Total charge and mass changing cross sections of relativistic nuclei in hydrogen, helium, and carbon targets, *Phys. Rev. C* **41**, 520 (1990).
- [38] R. E. Warner, R. A. Patty, P. M. Voyles, A. Nadasen, F. D. Becchetti, J. A. Brown, H. Esbensen, A. Galonsky, J. J. Kolata, J. Kruse, M. Y. Lee, R. M. Ronningen, P. Schwandt, J. von Schwarzenberg, B. M. Sherrill, K. Subotic, J. Wang, P. Zecher, Total reaction and $2n$ -removal cross sections of 20–60 A MeV $^{4,6,8}\text{He}$, $^{6-9,11}\text{Li}$, and ^{10}Be on Si, *Phys. Rev. C* **54**, 1700 (1996).
- [39] A. M. Sourkes, A. Houdayer, W. T. H. van Oers, R. F. Carlson, and R. E. Brown, Total reaction cross section for protons on ^3He and ^4He between 18 and 48 MeV, *Phys. Rev. C* **13**, 451 (1976).
- [40] M. S. Kozodaev, M. M. Kulyukin, R. M. Sulyaev, A. I. Filippov, and Y. A. Shcherbakov, Interactions between 630 MeV protons and ^4He nuclei, *Zh. Eksp. Teor. Fiz.* **38**, 708 (1960) [*Sov. Phys. JETP* **38**, 511 (1960)].
- [41] S. R. Neumaier, G. D. Alkhazov, M. N. Andronenko, A. V. Dobrovolsky, P. Egelhof, G. E. Gavrilov, H. Geissel, H. Irnich, A. V. Khanzadeev, G. A. Korolev, A. A. Lobodenko, G. Münzenberg, M. Mutterer, W. Schwab, D. M. Seliverstov, T. Suzuki, N. A. Timofeev, A. A. Vorobyov, and V. I. Yatsoura, Small-angle proton elastic scattering from the neutron-rich isotopes ^6He and ^8He , and from ^4He , at 0.7 GeV in inverse kinematics, *Nucl. Phys. A* **712**, 247 (2002).
- [42] J. C. Peng, R. M. DeVries, and N. J. DiGiacomo, Energy dependence of nucleus-nucleus total cross sections, *Phys. Lett. B* **98**, 244 (1981).
- [43] W. Shen, B. Wang, J. Feng, W. Zhan, Y. Zhu, and E. Feng, Total reaction cross section for heavy-ion collisions and its relation to the neutron excess degree of freedom, *Nucl. Phys. A* **491**, 130 (1989).
- [44] L. Sihver, M. Lantz, and A. Kohama, Improved parametrization of the transparency parameter in Kox and Shen models of total reaction cross sections, *Phys. Rev. C* **89**, 067602 (2014).
- [45] S. Agostinelli *et al.*, GEANT4 – A simulation toolkit, *Nucl. Instrum. Methods Phys. Res. A* **506**, 250 (2003).
- [46] H. Fuchs, J. Ströbele, T. Schreiner, A. Hirtl, and D. Georg, A pencil beam algorithm for helium ion beam therapy, *Med. Phys.* **39**, 6726 (2012).
- [47] B. Knäusl, H. Fuchs, K. Dieckmann, and D. Georg, Can particle beam therapy be improved using helium ions? A planning study focusing on pediatric patients, *Acta Oncol.* **55**, 751 (2016).
- [48] F. A. Cucinotta, L. W. Townsend, and J. W. Wilson, Description of alpha-nucleus interaction cross sections for cosmic ray shielding studies, NASA Technical Paper No. 3285, 1993.
- [49] J. W. Wilson, F. F. Badavi, F. A. Cucinotta, J. L. Shinn, G. D. Badhwar, R. Silberberg, C. H. Tsao, L. W. Townsend, and R. L. Tripathi, HZETRN: Description of a free-space ion and nucleon transport and shielding computer program, NASA Technical Paper No. 3495, 1995.
- [50] M. Durante and F. A. Cucinotta, Physical basis of radiation protection in space travel, *Rev. Mod. Phys.* **83**, 1245 (2011).
- [51] J. W. Norbury, J. Miller, A. M. Adamczyk, L. H. Heilbronn, L. W. Townsend, S. R. Blattnig, R. B. Norman, S. B. Guetersloh, and C. J. Zeitlin, Nuclear data for space radiation, *Radiat. Meas.* **47**, 315 (2012).